Electronic Supplementary Material (ESI) for Soft Matter.

Supplemental Information

Nondestructive Characterization of Soft Materials and Biofilms by Measurement of Guided Elastic Wave Propagation Using Optical Coherence Elastography

Hong-Cin Liou[1], Fabrizio Sabba[2], Aaron Packman[2], George Wells[2], Oluwaseyi Balogun[1,2]*

[1]Mechanical Engineering Department, Northwestern University, Evanston, IL 60208

[2]Civil and Environmental Engineering Department, Northwestern University, Evanston, IL 60208

***Corresponding author:**

Oluwaseyi Balogun, Phone: +1 847-491-3054; e-mail: o-balogun@u.northwestern.edu

The following are included as supplemental information for this paper:

Number of pages: 8

Number of supplementary sections: 5

Number of figures: 4

S1 – Agar preparation protocol

The following states the steps of preparation for gels of 1% and 2% agarose concentration.

(1) Pour 100ml nanopurified water (94 mL) and skim milk solution (6 mL) into a 250 mL Pyrex glass bottle;

(2) Add agarose powders to the solution. Prevent any powder from attaching to the inner bottle wall above the solution surface;

(3) Apply the cap to the bottle and boil the solution using a microwave oven. Cap must not be fully sealed to allow pressure release when the solution is being boiled. Turn off the microwave immediately once bubbles form due to vicious boiling;

(4) Remove bottle from the microwave oven and gently shake to allow mixing of undissolved powder;

(5) Reheat the solution for a thorough boiling and mixture;

(6) After reheating the solution, completely seal the cap to prevent any moisture loss. The bottle is then shaken for 10 seconds to uniformly dissolve agar;

(7) Cool off the bottle at room temperature for 20 minutes. Tilt the bottle so that the condensed water can go back into solution;

(8) Pour the solution in the final container and place in the water bath;

(9) Cover the containers to eliminate moisture loss and leave them at room temperature for 90 minutes until the agarose gels are fully solidified;

(10) Place the agarose gels in the water bath until experiment to prevent moisture loss.

(11) Wait 8 hours before performing any experiment to allow complete development of cross-linking in the gels.

S2 – The effect of the time delay *dt* to the OCE images

The phase-sensitive OCT can record the optical phase $\varphi(x,z,t)$ of the light scattered back from the sample at a spatial location (x,z) at time t and relate the phase difference $\Delta\varphi$ from two adjacent A-scans to the difference of local axial displacements $u_z(x,z,t)$. For example, suppose the first A-scan is recorded at time t_o and location x_o, corresponding to the optical phase $\varphi(x_o,z,t_o)$ and axial displacement $u_z(x_o,z,t_o)$. Then, the second A-scan is recorded at time $t_o + dt$ and location $x_o + dx$ where dt is a time delay and dx is the spatial scanning step of the OCT. Note that the spatial scanning step (4μm) is much smaller than the shortest wavelength we measured ($380\mu m$), so that we can assume $x_o + dx \cong x_o$, meaning the two A-scans are recorded approximately at the same x location. Therefore, the associated optical phase and displacement of the second A-scan are $\varphi(x_o,z,t_o + dt)$ and $u_z(x_o,z,t_o + dt)$. The phase difference and the displacement difference of the two A-scans are

$$\Delta\varphi(x_o,z,t_o) = \varphi(x_o,z,t_o + dt) - \varphi(x_o,z,t_o) \tag{S1}$$

and

$$\Delta u_z(x_o,z,t_o) = u_z(x_o,z,t_o + dt) - u_z(x_o,z,t_o) \tag{S2}$$

From the theory, $\Delta\varphi$ and Δu_z have the relation such that

$$\Delta\varphi(x_o,z,t_o) = 4\pi n(x_o,z)\Delta u_z(x_o,z,t_o)/\lambda_o \tag{S3}$$

where $n(x,z)$ is the local index of refraction of the sample, and λ_0 is the center wavelength of the OCT light source.

In our measurements, the local displacement induced by the elastic wave with a single frequency ω can be expressed as

$$u_z(x,z,t) = A(x,z)sin(\omega t) \tag{S4}$$

where $A(x,z)$ is the space-dependent amplitude. Then, the displacement difference over the time delay dt is

$$\Delta u_z(x_o,z,t_o) = A(x,z)[\sin(\omega(t+dt)) - \sin(\omega t)] = 2A(x,z)\sin\left(\frac{\omega dt}{2}\right)\cos\left(\omega t + \frac{\omega dt}{2}\right) \tag{S5}$$

which shows that the displacement difference Δu_z is also a combination of amplitude and time-dependent harmonic function. The amplitude term $2A(x,z)\sin\left(\frac{\omega dt}{2}\right)$ will reach its maximum when $\omega dt = (4m+1)\pi$ and vanish when $\omega dt = 2m\pi$ as $m = 0,1,2,3,\ldots$.

Figure S1 shows the measurements at the same driving frequency ω with three different dt where $\omega dt = 0.3\pi$, π, and 2π. Note that the value of the phase difference $\Delta\varphi$ ranges from $-\pi$ to π, but the color variation in the figures is set to only change within $\Delta\varphi = [-\pi/2, \pi/2]$ to enhance the color contrast. Also, because $\Delta\varphi$ only ranges from $-\pi$ to π, when a $\Delta\varphi$ value is larger than π, say 1.1π, it will flip over to the negative region and become -0.9π. This phenomenon is called phase wrapping. An example of phase wrapping is shown in Fig. S1a indicated by a dash-lined rectangle where the blue area should have the same sign with the surrounding red area.

Comparing Fig. S1a and S1b, several observations can be made. (1) The wave patterns have the same spatial variation throughout the field of view except a phase shift. The spatial variation is due to the same amplitude function $2A(x,z)\sin\left(\frac{\omega dt}{2}\right)$, and the phase shift results from the term $\frac{\omega dt}{2}$ in the cosine function. The relevant wave patterns are indicated by the arrows between the figures. (2) For Fig. S1b, since $\omega dt = \pi$, leading to the maximum of the amplitude term $2A(x,z)\sin\left(\frac{\omega dt}{2}\right)$, the wave patterns in Fig. S1b have stronger phase wrapping than those in S1a. (3) The wave pattern is noisier in Fig. S1b than in S1a because a longer time delay would introduce more random background noise. On the other hand, there is no wave pattern in Fig. S1c, which validates the relation that $\Delta u_z = 0$ when $\omega dt = 2\pi$.

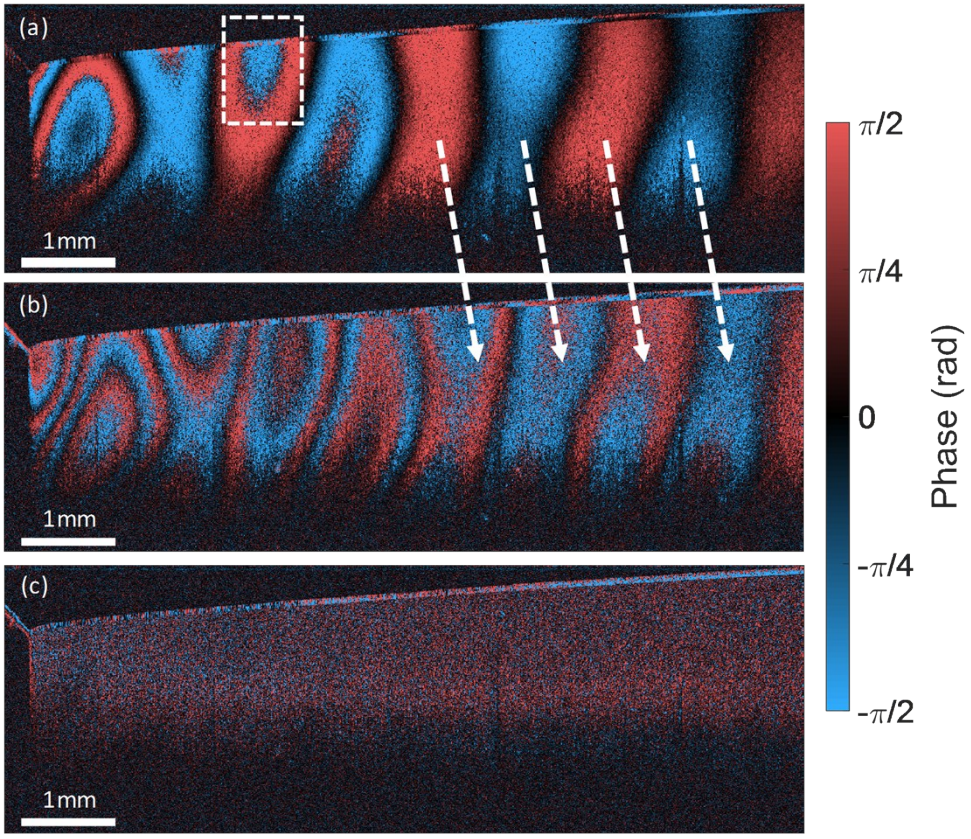

Fig. S1. Wave patterns in OCE images corresponding to different ωdt. (a) $\omega dt = 0.3\pi$, (b) $\omega dt = \pi$, and (c) $\omega dt = 2\pi$.

S3 – Characterization of the frequency-dependent response of the paddle actuator

The paddle actuator, composed of an 18-gauge syringe needle and a 10 mm wide razor blade glued on the end of the needle, is attached to a piezoelectric transducer (Thorlabs PZS001) driven by a sinusoidal voltage from a radio frequency function generator (Agilent 33120A, CA, USA). Since the local excitation of the longitudinal and shear elastic waves at different frequencies depends on the axial vibration of the actuator, it is important to investigate its dynamic responses within the frequency span.

The dynamic response is characterized using the knife-edge technique as illustrated in Fig. S2a. A laser beam with constant beam width is guided directly to a photodetector which converts the detected intensity

of the laser light to electric signal displayed on an oscilloscope. The laser beam is partially blocked by the edge of the razor blade so that the axial vibration of the actuator would cause the intensity variation of the laser beam that arrives at the photodetector. The peak-to-peak voltage, associated with the relative amplitude of the axial displacement, is recorded from the oscilloscope reading at every sampling frequency as shown in Fig. S2b. The result shows that three resonant frequencies (200 Hz, 2000 Hz, and 5800 Hz) and a relative low-response region (1800-1900 Hz) are embedded in a moderate decreasing trend along the frequency. We note that sufficient vibration can be observed over the whole frequency span of interest, which validates the use of the paddle and the driving circuit as the actuator for wave generation.

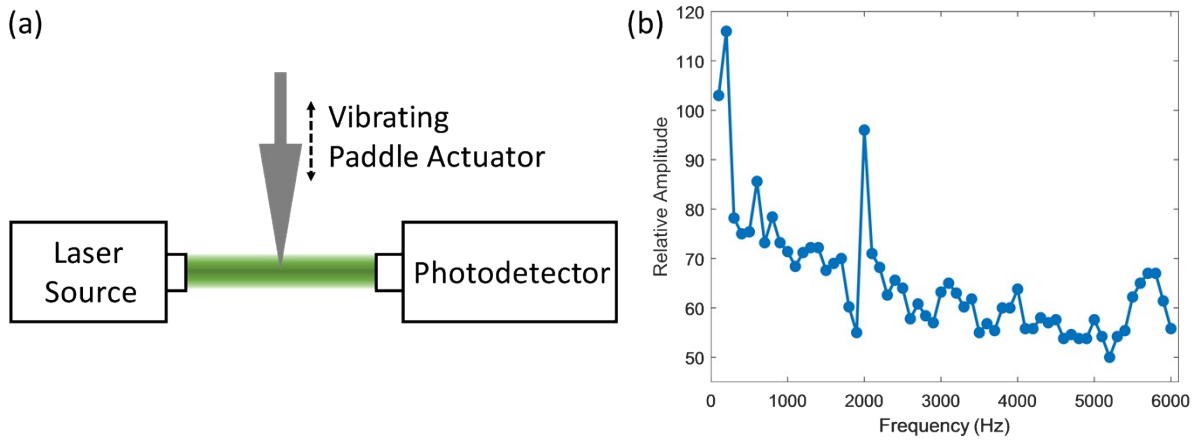

Fig. S2. (a) Configuration of the knife-edge technique for dynamic response characterization, and (b) Relative amplitude of the axial displacement of the paddle actuator at different frequencies.

S4 – Hybrid path for estimating the elastic wavelengths in the biofilm

The OCE B-scan (Fig. 8b) shows a clear evidence that the elastic wave propagation is affected by the surface curvature of the biofilm; therefore, we adapted a hybrid path to estimate the elastic wavelengths. This leads to a more precise calculation of the elastic wave speeds compared to using solely a straight-line path. As shown in Fig. S3, the path contains an initial curve that follows the surface topography within the

first 2 mm of the biofilm lateral extent and a following straight line where the surface roughness is negligible. The curve was obtained by image processing algorithms including edge-detection and curve-fitting with a cubic function. The amplitudes of the elastic waves at discrete intervals along the dashed line were extracted, and fast Fourier transform was applied to obtain the spatial frequency (or inverse wavelength) of the elastic waves. The discrete intervals along the path were resized equally in the curve and straight-line parts to meet the requirement of fast Fourier transform.

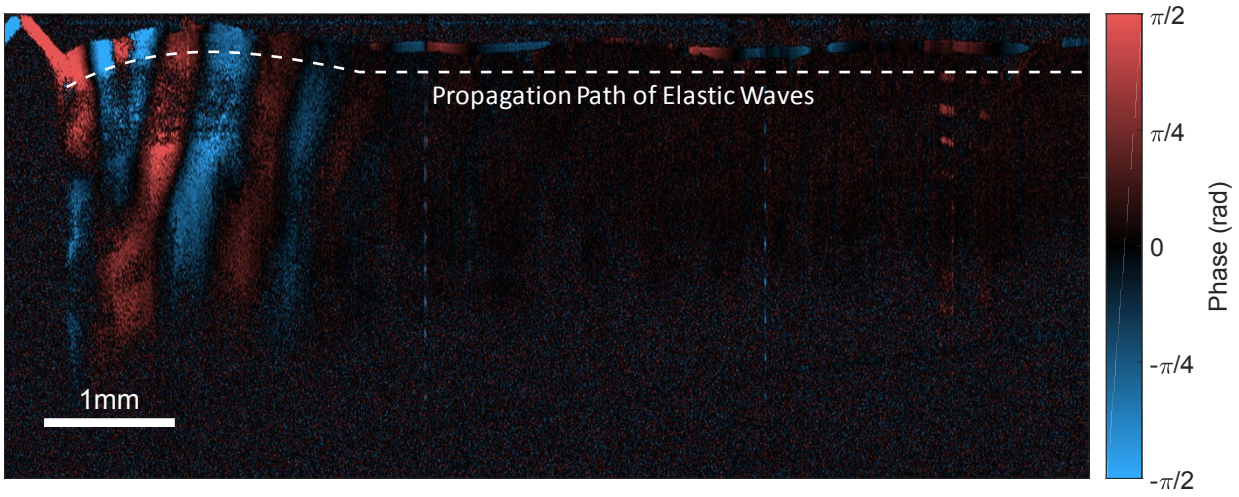

Fig. S3. The hybrid path (white dashed line) used to estimate the elastic wavelength in the biofilm.

S5 – Rheometer measurements on 1 mm and 10 mm thick 2.0% agarose gel samples

A group of independent measurements using a Rheometer (Anton Paar MCR 302) was performed to obtain the complex shear modulus and viscosity in the 1 mm and 10 mm thick 2.0% agarose gel samples. The Rheometer experiments were conducted with the parallel plates configuration which used an upper rotating plate (diameter = 15 mm) that was in contact with sample's top surface to apply a torsional shear load on the sample. The sample was placed on a fixed lower plate, and its responses to the shear load were recorded to calculate the complex shear modulus and viscosity. The plates were operated under the Frequency Sweep Mode which recorded the complex shear modulus and viscosity at various angular frequencies of the

rotating plate from 1 rad/s to 100 rad/s at a constant shear strain = 0.03%. The results of the shear modulus and viscosity are plotted in Fig. S4a and S4b, respectively. Each data point and error bar correspond to the mean value and the standard deviation from repeated measurements on three separate samples. From Fig. S4a, the averaged shear moduli for 1 mm and 10 mm thick samples over the angular frequency range from 1 rad/s to 10 rad/s where the data points remain relatively constant are 12.6 kPa and 9.1 kPa. The value 12.6 kPa of the 1 mm sample has extremely excellent agreement with our OCE measurements listed in Table 1, and the value 9.1 kPa of the 10 mm sample is within the same order. This suggests that the OCE technique has high accuracy on estimating the shear moduli of soft materials. The results in Fig. S4b show that 1 mm and 10 mm thick agarose gels have comparable viscosities for angular frequency less than 40 rad/s. Beyond this frequency, the viscosity of the 10 mm sample is noticeably larger than that of the 1 mm sample. We remark that the lowest angular frequency of our OCE measurements on agarose samples was 6283 rad/s (1 kHz), which is significantly higher than the frequency range of the rheometer measurements. Nevertheless, the rheometer measurements suggest that the 10 mm thick sample has a larger viscosity compared to the 1 mm thick sample of the same composition, as observed in our OCE measurements.

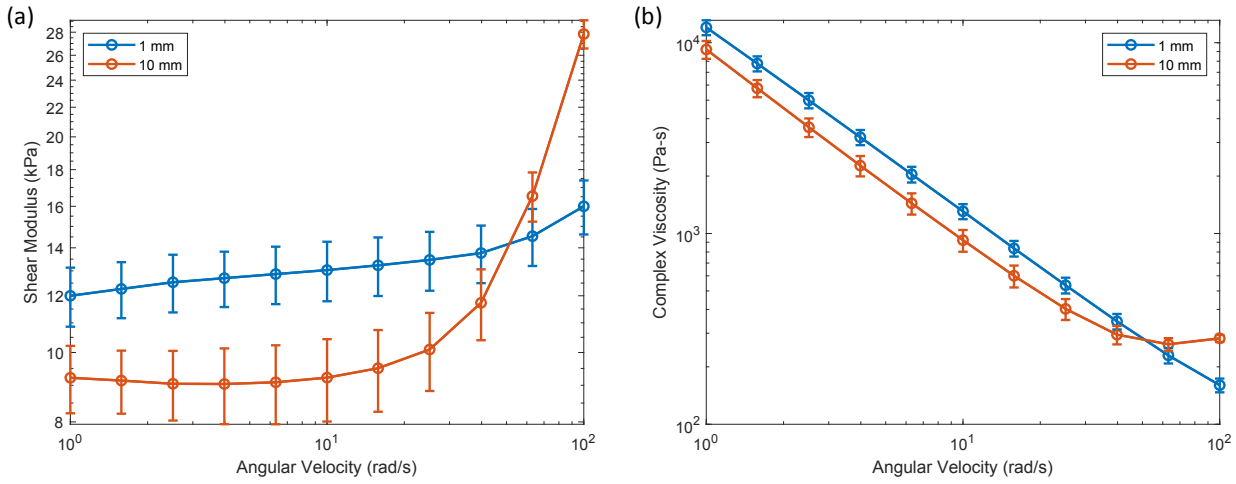

Fig. S4. The results of Rheometer measurements: (a) shear modulus and (b) complex viscosity.